Journal of Solid State Chemistry **147,** 464–477 (1999)
Article ID jssc.1999.8384, available online at http://www.idealibrary.com on IDEAL®

# Structure and Magnetism of $Pr_{1-x}Sr_xCoO_{3-\delta}$

H. W. Brinks,* H. Fjellvåg,* A. Kjekshus,*,[1] and B. C. Hauback†

*Department of Chemistry, University of Oslo, P.O. Box 1033, Blindern, N-0315 Oslo, Norway; and †Institute for Energy Technology, N-2007 Kjeller, Norway

Received January 20, 1999; in revised form April 27, 1999; accepted May 21, 1999

**The structural, magnetic, and nonstoichiometric properties of the perovskite-like $Pr_{1-x}Sr_xCoO_{3-\delta}$ phase ($0 \le x \le 0.80$) have been studied by powder X-ray and neutron diffraction and magnetic susceptibility measurements between 5 and 295 K as well as by redox titration. In the compostion range $0 \le x \le 0.30$ the structure can be described with a $GdFeO_3$-type atomic arrangement (space group *Pnma*), while the structure in the composition range $0.30 < x \le 0.80$ involves a lower symmetry (space group $P2_1/n$). Samples with $0.10 \le x \le 0.80$ exhibit ferromagnetism below a Curie temperature of $\le 250$ K, depending on the composition. The $Pr_{1-x}Sr_xCoO_{3-\delta}$ phase behaves as a relatively hard magnetic material. For samples prepared and cooled to room temperature in air, the oxidation state of cobalt increases linearly up to $x \approx 0.50$ and stabilizes at +3.4 for higher substitution levels of Sr. On the basis of the present data, it is not possible to prove or disprove that there occurs charge ordering in $Pr_{1-x}Sr_xCoO_{3-\delta}$.** © 1999 Academic Press

## I. INTRODUCTION

A large number of compounds with the perovskite-type structure or closely related variants thereof have over the years received considerable attention, owing to their interesting chemical and physical properties. More recently, the focus has shifted from structural features and phase transitions to more exotic properties like high-temperature superconductivity, colossal magnetoresistance, cooperative magnetism with high transition temperatures, high ionic conductivity, and pronounced catalytic properties. However, a perplexing aspect is that most of these rather special properties to a large extent is element-specific, high-temperature superconductivity associated with copper, colossal magnetoresistance with manganese, and cooperative magnetism with high transition temperatures with iron, whereas high ionic conductivity and catalytic features are less element-specific.

The present paper focuses on crystal structure, oxygen nonstoichiometry, and magnetic properties of $Pr_{1-x}Sr_xCoO_{3-\delta}$. In the literature there exist some reports on its electrical conductivity (1–3) and certain structural properties (2–4). However, the latter are burdened with uncertainties, owing to the lack of proper determination of coordinates for the oxygen atoms, by, e.g., neutron diffraction. The related phase $La_{1-x}Sr_xCoO_{3-\delta}$ has been subjected to extensive studies in the search for colossal magnetoresistance (5, 6) and for possible applications as a sensor (7), oxygen membrane (8, 9), solid oxide fuel cell (10), and catalysts (11). The present work on $Pr_{1-x}Sr_xCoO_{3-\delta}$ focuses *inter alia* on the following interesting aspects: (i) A possible correlation between the crystal structure and the change in the electric conductivity around $x = 0.30$; (ii) the possibility of $Co^{3+}$ and $Co^{4+}$ (formal charges) charge ordering (CO) for $Pr_{1-x}Sr_xCoO_3$ with $x \approx 0.50$; (iii) change from diamagnetic low-spin (LS) $Co^{3+}$ for $x = 0$ to dia-, para-, ferromagnetic mixed valent $Co^{3+}/Co^{4+}$ states for larger $x$; (iv) redox behavior of grossly nonstoichiometric Sr-rich samples.

## II. EXPERIMENTAL

### *Synthesis*

$Pr_6O_{11}$ (99.9%, Strem Chem.) was dissolved in hot diluted nitric acid (p.a., Riedel de Haën). $SrCO_3$ (98%, Fluka), $Co(NO_3)_2 \cdot 6H_2O$ (99%, Fluka) and excess citric acid monohydrate (99.5%, Riedel de Haën; 5–10 times the molar amount of the cations) were added, and the solution was heated at 180°C overnight. The resulting xerogel is X-ray amorphous. The xerogel was fired at 350°C to remove a major part of the carbonaceous species. This precursor was pressed in tablets and crystallization was carried out in an alumina container at 900°C in air. Prior to the weighing for the synthesis, $Pr_6O_{11}$ and $SrCO_3$ were heat-treated at 430°C in air to remove the adsorbed water. The metal content of the cobalt nitrate hydrate was determined gravimetrically by complete decomposition to $Co_3O_4$. All samples were phase-pure according to powder X-ray diffraction (PXD). Characterization by differential scanning calorimetry (DSC) showed upon heating an endothermic peak at $\sim 150$°C for samples with $0.10 \le x \le 0.50$, but this effect could most probably, on the basis of thermogravimetric

[1] To whom correspondence should be addressed.



0022-4596/99 $30.00

(TG) and PXD data, be attributed to loss of adsorbed water.

Some samples were after crystallization heated under an enhanced oxygen pressure at 450°C. This was done in a silica-glass container which was contained in an iron autoclave placed in a vertical tube furnace. The autoclave was connected via a thin stainless steel tube directly to an oxygen bomb; thereby, the oxygen pressure range from ambient to ca. 200 bar was covered.

### *Powder X-Ray Diffraction (PXD)*

PXD data were collected with a Siemens D5000 diffractometer equipped with a primary Ge monochromator, position-sensitive detector, and using Cu$K\alpha_1$ radiation and Si as the internal standard. Unit-cell dimensions were determined by least-squares refinements using the UNITCELL program (12). Simulation of PXD patterns were carried out with the LAZY PULVERIX program (13).

High-temperature data up to 900°C were collected in air with a Siemens D500 diffractometer equipped with a secondary monochromator and scintillation counter. The sample was placed directly on a platinum resistance filament.

### *Powder Neutron Diffraction (PND)*

PND data were collected with the two-axis diffractometer PUS at the JEEP II reactor, Kjeller, Norway. Monochromatized neutrons of wavelength $\sim 155$ pm were obtained by reflection from Ge (511) and detected by two banks with position-sensitive detectors, each covering 20° in $2\theta$. The data sets consisted of 2400 measured intensity points. Low temperatures were obtained by means of a Displex cooling system.

Rietveld refinements were performed using the FULLPROF98 version 0.2 (14), taking scattering lengths from the library of the program. A pseudo-Voigt profile function was used for the PND and PXD data. Isotropic temperature factors were refined for the different types of atoms. No absorption correction was made, which may be the cause of low and, in a few cases, even negative temperature factors. However, the lacking correction is considered to have no significant effect on unit-cell dimensions and atomic coordinates. Typical values for the temperature factors (in $10^4$ pm$^2$) at 295 K are $B_{Pr,Sr} = 0.50$, $B_{Co} = 0.20$, and $B_O = 0.60$.

### *Magnetization*

Magnetization data were measured with an MPMS (Magnetic Property Measurement System; Quantum Design). Data were collected between 5 and 300 K for (15–40 mg) samples subjected to zero-field-cooled (ZFC) or field-cooled (FC) conditions (45 kOe). A measure for the Curie temperature ($T_C$) was obtained by extrapolation of the inflection point of the magnetization curve to the temperature axis. This gives a too high $T_C$, but this method was regarded as an adequate method for comparison of different samples. By determination of the saturation magnetization, the paramagnetic contribution from $Pr^{3+}$ was subtracted from the observed magnetization to get hold of the Co contribution. The $Pr^{3+}$ contribution was determined from $PrCoO_3$, which is expected to carry paramagnetic contributions from only $Pr^{3+}$ at low temperatures.

$PrCoO_3$ was furthermore measured between 295 and 970 K by means of the Faraday method (12 mg, 0–8 kOe field).

### *Thermal Analyses*

Thermogravimetric (TG) data were collected with a Perkin–Elmer 7 series instrument. Silica-glass containers were used as sample holders. DSC data were obtained with a Mettler DSC 3000 system.

### *Oxygen Analysis*

The oxidation state of cobalt was determined by iodometric titration in an argon atmosphere after dissolution of the sample in HCl in a closed, argon-flushed glass container. KI was added prior to the dissolution and was oxidized by the sample to $I_2$, which was titrated with a $S_2O_3^{2-}$ solution. This solution was adjusted with $KIO_3$. Three or more parallels were used, and the standard deviation for the oxygen content was typically 0.002.

## III. RESULTS

### (*i*) *Solid-Solution Range and Crystal Structure of $Pr_{1-x}Sr_xCoO_{3-\delta}$ at 295 K*

The $Pr_{1-x}Sr_xCoO_{3-\delta}$ solid-solution phase with a perovskite-like structure exists for $0 \le x \le 0.80$ at 295 K. By visual inspection of the diffractograms, there seems to be a rather abrupt change in the structure around $x = 0.30$. For Sr levels above $x = 0.80$, $Co_3O_4$ and $Sr_6Co_5O_{15}$ are observed. The end member $SrCoO_3$ decomposes upon cooling to room temperature into $Sr_6Co_5O_{15}$ and $Co_3O_4$ (15). The compositional variation of the unit-cell dimensions (as determined by PXD) is shown in Fig. 1.

There are different structural distortions of the ideal perovskite-type structure throughout the solid-solution range, as evident by visual inspection of the collected PXD and PND patterns. The tilting of the octahedra were evaluated on the basis of the symmetry considerations of Glazer (16) and Woodward (17). In addition to the tilts, which are accompanied by slight shifts in the position of the *A*-site elements (Pr and Sr), the possibility of *B*-site ordering

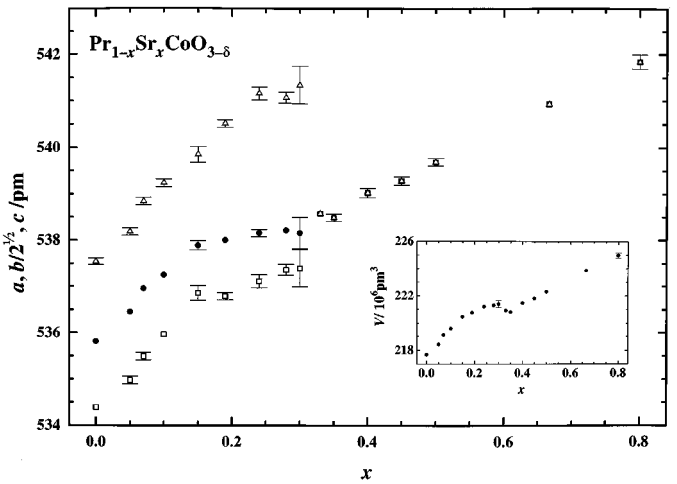


**FIG. 1.** Unit-cell dimensions ($a$, squares; $b/\sqrt{2}$, circles; $c$, triangles) for $Pr_{1-x}Sr_xCoO_{3-\delta}$ as a function of composition $x$, determined by PXD. Inset: Unit-cell volume as a function of $x$.

originating from different Co species, in particular, at low temperature, was considered. A minus tilt of the $BO_6$ octahedra (according to the Glazer notation) implies superstructure reflections of the type $N = h^2 + k^2 + l^2 = 4C + 3$, $C$ being an integer, for a $2a_p \times 2a_p \times 2a_p$ ("doubled") unit-cell, $a_p$ being the unit-cell dimension of a corresponding hypothetical cubic perovskite. A plus tilt implies extra reflections of the type $N = 4C + 2$. Two minus tilts result in a monoclinically deformed doubled perovskite cell, and three minus tilts imply a triclinic cell. For $Pr_{1-x}Sr_xCoO_{3-\delta}$ extra reflections caused by minus and plus tilts are observed by PXD for samples with $x < 0.30$. Moreover, the splitting of $\{2\,2\,2\}$ and $\{4\,4\,4\}$ for the doubled cell indicates at least two minus tilts. With two minus tilts and one plus tilt, there are two possible structure models, specified either in space group *Pnma* or $P2_1/m$, both with $a \approx \sqrt{2}a_p$, $b \approx 2a_p$, and $c \approx \sqrt{2}a_p$. The Rietveld refinements gave approximately equal reliability factor for both descriptions, and *Pnma* was favored, owing to its higher symmetry. For $0 \le x \le 0.30$ the structure is hence considered to be of the orthorhombic $GdFeO_3$ type. Results from Rietveld refinements of PND data for $PrCoO_3$ (295 K) and $Pr_{0.80}Sr_{0.20}CoO_{2.99}$ (295 and 10 K) are given in Table 1.

At first sight the Bragg reflections for $0.30 \le x \le 0.80$ appear not to be split, and the PXD data could be indexed on a cubic unit cell (Fig. 1). However, a closer examination of the peak profiles clearly revealed shoulders indicative of lower symmetry. For $x > 0.30$, plus tilts are not observed with PXD and minus tilts only when very long counting times were used. However, PND for $x = 0.50$ (Fig. 2) reveals both plus and minus tilts. Furthermore, both PXD and PND indicate that $\{4\,4\,4\}$ is split into three separate parts (Fig. 3), which according to Glazers considerations should imply three minus tilts. However, three minus tilts and one plus tilt are physically impossible. A possible unit cell which appropriately indexes the reflections is $a \approx \sqrt{2}a_p$, $b \approx \sqrt{2}a_p$, and $c \approx \sqrt{2}a_p$ with space group $P2_1/n$ (standard setting $P2_1/c$ with $a \approx 2a_p$, $b \approx \sqrt{2}a_p$, $c \approx \sqrt{6}a_p$, and $\beta \approx 145°$). This description implies two nonequivalent cobalt positions (17).

Kharton and Demin (2) indexed their PXD patterns of $Pr_{1-x}Sr_xCoO_{3-\delta}$, $0 \le x \le 0.50$, according to a doubled cubic unit cell and attributed the doubling of the axes to "ordering of the oxygen sublattice," neglecting the fact that such doubled unit cells should be monoclinic rather than cubic, according to the symmetry considerations of Glazer (16). This is clearly seen by the splitting of $\{2\,2\,2\}$. The present diffraction data can only to a limited extent be indexed on such a cubic unit cell. All studies (present, 2, 3) agree that the unit-cell volume per formula unit ($V/Z$) increases with $x$. However, the $V/Z$ data in Refs. (2, 3) are systematically lower than the present ones. For $Pr_{1-x}Sr_xCoO_{3-\delta}$ with $x \le 0.15$, Kostogloudis *et al.* (3) agree on the $GdFeO_3$-type structure attributed here. The discrepancy in $V/Z$ may either reflect differences in indexing or be caused by different oxygen contents in the samples of Kostogloudis *et al.* (3).

### (*ii*) *Crystal Structure of* $Pr_{0.50}Sr_{0.50}CoO_{2.965}$

The crystal structure of $Pr_{0.50}Sr_{0.50}CoO_{2.965}$ was refined according to the Rietveld method (PND data) in space group $P2_1/n$ (*vide supra*) and a satisfactory fit ($\chi^2 = 2.2$ for the 295 K data) was obtained. The only significant misfit was a weak, unexplained reflection at $2\theta = 74.5°$ ($\lambda = 1.5492$ Å). Results based on PND data at 10, 170, and 295 K are given in Table 2. Although the line splitting is small

**TABLE 1**

**Structural Parameters for $Pr_{1-x}Sr_xCoO_{3-\delta}$ with $x = 0$ ($\delta = 0$) and 0.20 ($\delta = 0.01$) According to Rietveld Refinements of PND Data (Space Group *Pnma* with Pr/Sr in 4*c*, Co in 4*a*, O(1) in 4*c*, and O(2) in 8*d*; Calculated Standard Deviations in Parentheses)**

| $x$, $T$ ($K$) | 0, 295 | 0.20, 295 | 0.20, 10 |
|---|---|---|---|
| $a$ (pm) | 534.03(2) | 536.49(2) | 535.08(2) |
| $b$ (pm) | 757.44(2) | 760.62(3) | 757.39(1) |
| $c$ (pm) | 537.54(2) | 540.89(2) | 539.51(2) |
| $x_{Pr/Sr}$ | 0.4721(5) | 0.4806(5) | 0.4782(4) |
| $z_{Pr/Sr}$ | − 0.0046(7) | − 0.0033(6) | − 0.0021(4) |
| $x_{O1}$ | 0.0056(5) | 0.0047(5) | 0.0057(4) |
| $z_{O1}$ | 0.0675(4) | 0.0599(4) | 0.0628(3) |
| $x_{O2}$ | 0.2824(3) | 0.2758(3) | 0.2767(2) |
| $y_{O2}$ | − 0.0359(2) | − 0.0318(2) | − 0.0326(1) |
| $z_{O2}$ | 0.2180(3) | 0.2251(3) | 0.2230(2) |
| $\mu_F/\mu_B$ | — | — | 0.85(3) |
| $R_P$ | 0.048 | 0.048 | 0.038 |
| $\chi^2$ | 2.03 | 1.11 | 1.72 |

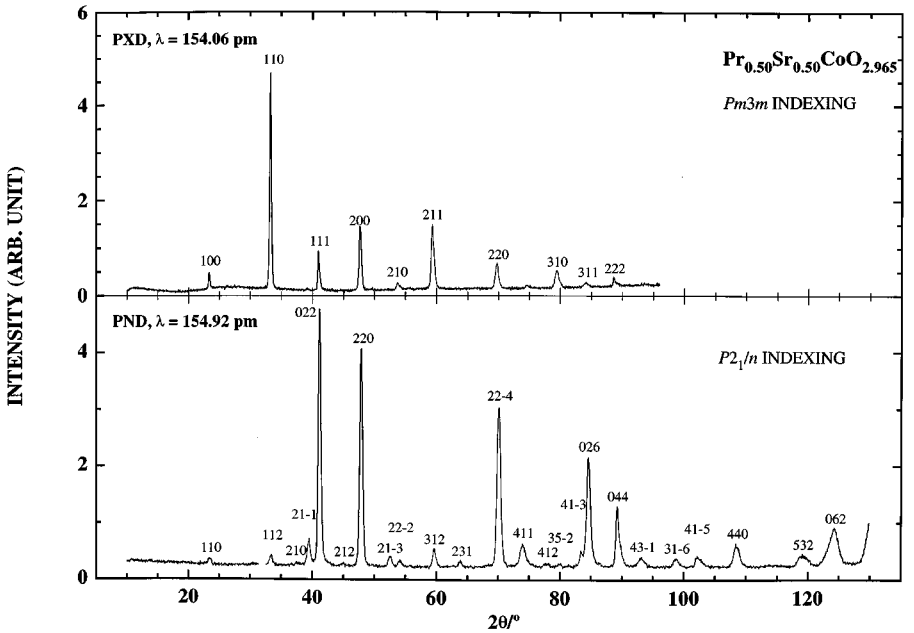


**FIG. 2.** Comparison of PXD (top) and PND (bottom) profiles for $Pr_{0.50}Sr_{0.50}CoO_{2.965}$ (collected with approximately the same wavelength). The PXD pattern shows indexing according to the parent cubic perovskite, while the PND pattern reveals superstructure reflections due to a larger unit cell, indexed in space group $P2_1/n$.

owing to the pseudo-cubic metric ($a/\sqrt{2} \approx b/\sqrt{2} \approx c/2 \approx a_p$), the PND data clearly show an anomalous change in the unit-cell dimensions between 10 and 170 K, where $c$ decreases by 0.32%, while $a$ and $b$ increase, giving an overall increase in the volume of 0.14%. These changes are probably of a magnetic origin (*vide infra*). Because of the

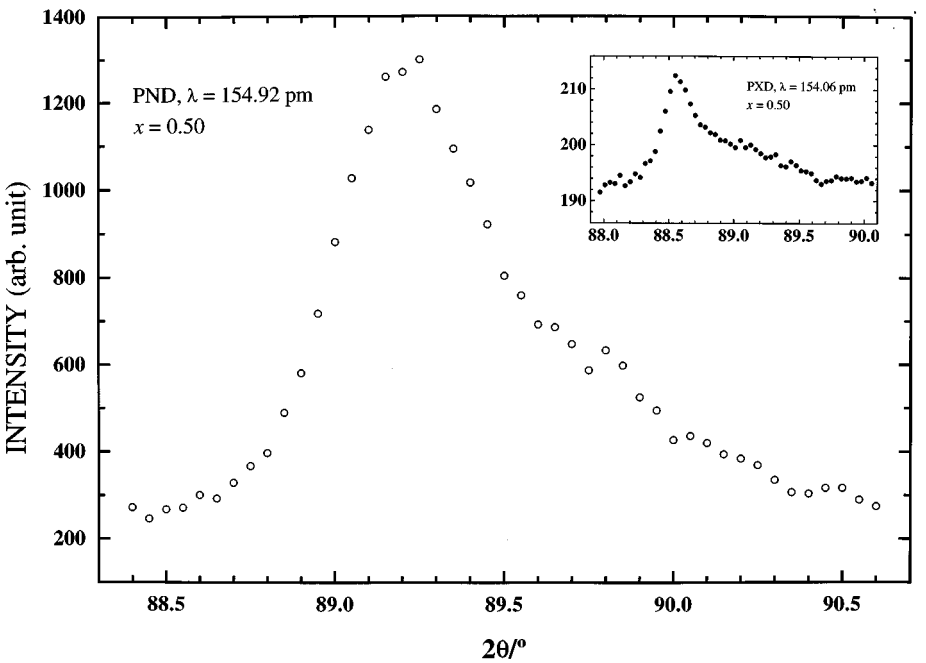


**FIG. 3.** Splitting of {444} for the doubled perovskite into three parts with an intensity ratio of approximately 3:1:1 [(044), (40$\bar{4}$), (404)] for $Pr_{0.50}Sr_{0.50}CoO_{2.965}$. PND and PXD (inset) data shown.

**TABLE 2**
**Structural Parameters for $Pr_{0.50}Sr_{0.50}CoO_{2.965}$ According to Rietveld Refinements of PND Data (Space Group $P2_1/n$ with Pr/Sr in 4*e*, Co(1) in 2*c*, Co(2) in 2*d* and O(1), O(2), and O(3) in 4*e*; Calculated Standard Deviations in Parentheses)**

| $T$ (K) | 295 | 170 | 10 |
|---|---|---|---|
| $a$ (pm) | 537.51(6) | 536.53(6) | 535.21(6) |
| $b$ (pm) | 539.93(5) | 538.29(5) | 537.11(5) |
| $c$ (pm) | 764.87(7) | 763.34(7) | 765.78(6) |
| $\beta$ (°) | 90.308(8) | 90.339(8) | 90.21(1) |
| $x_{Pr/Sr}$ | 0.017(1) | 0.017(2) | 0.025(1) |
| $y_{Pr/Sr}$ | −0.005(2) | 0.000(3) | −0.006(2) |
| $z_{Pr/Sr}$ | 0.243(1) | 0.245(1) | 0.246(2) |
| $x_{O1}$ | 0.275(2) | 0.270(3) | 0.272(3) |
| $y_{O1}$ | 0.268(2) | 0.261(3) | 0.268(3) |
| $z_{O1}$ | 0.011(2) | 0.011(2) | 0.015(2) |
| $x_{O2}$ | 0.255(2) | 0.257(2) | 0.251(2) |
| $y_{O2}$ | 0.253(2) | 0.258(3) | 0.260(3) |
| $z_{O2}$ | 0.493(2) | 0.488(2) | 0.499(2) |
| $x_{O3}$ | 0.5509(10) | 0.5527(10) | 0.5523(10) |
| $y_{O3}$ | −0.007(3) | −0.005(4) | −0.010(3) |
| $z_{O3}$ | 0.246(1) | 0.249(1) | 0.262(2) |
| $\mu_F/\mu_B$ | — | 1.12(10) | 1.42(10) |
| $R_P$ | 0.059 | 0.056 | 0.072 |
| $\chi^2$ | 2.26 | 7.85 | 3.31 |

recognized instability of $Co^{4+}$ (18), oxygen occupation numbers enter as additional structural variables for $x > 0$. However, for $x = 0.50$ with an oxygen content of 2.965 (as determined by redox titrations) the vacancy concentration was too low to be detected in the PND data.

In space group $P2_1/n$ there are two nonequivalent Co atoms. One may envisage the existence of different Co species; i.e., for the composition $Pr_{0.50}Sr_{0.50}CoO_{2.965}$ one may have a $Co^{3+}d^6$ LS species and another $Co^{4+}$ species. Actually, this situation could apply to the entire $Pr_{1-x}Sr_xCoO_{3-\delta}$ solid-solution range, although there are no observed indications of a symmetry reduction in the PND data for $x = 0.20$.

For $x = 0.80$ no superstructure reflections were observed by PXD, and the main reflections were only slightly asymmetric. PND data revealed only one superstructure reflection. The splitting of $\{8\,0\,0\}$ according to a doubled cell, along with some asymmetric reflections, indicate a symmetry lower than cubic. The evolution with $x$ of the cell parameters refined according to $P2_1/n$ are shown in Fig. 4.

For the purpose of comparison, unit-cell dimensions and positional parameters for $0 \leq x \leq 0.30$ were refined according to space group $P2_1/n$ (PND and PXD data). No discrepancies were encountered with respect to the results presented above for space group *Pnma*. Figure 4 shows that $a$ decreases markedly above $x = 0.30$, while $b$ and $c$ increase markedly less pronounced. Hence, $x \approx 0.35$ will appear in PXD patterns as cubic, whereas for $x \geq 0.40$ distinct line splittings are again observed.

Selected interatomic distances and angles for $x = 0$, 0.20 (*Pnma*), and 0.50 ($P2_1/n$) are compared in Table 3. The listed coordination numbers for Pr/Sr refer to bond distances corresponding to bond valences larger than $0.038v_{Pr/Sr}$ [$v$ denotes valence; see the arguments in Ref. (19)]. When $x$ is increased, the average Pr/Sr coordination is significantly altered, from a deformed monocapped square antiprism (CN = 9) for $x = 0$ to a cuboctahedron (CN = 12) for $x = 0.50$. This clearly originates from the larger size of $Sr^{2+}$ (131 pm) compared to $Pr^{3+}$ (117.9 pm). When the size of Pr/Sr increases, there is space for more $O^{2-}$ (140 pm) around, which means that the structure is heading toward the ideal perovskite arrangement with close packing of $(Pr/Sr)O_3$ layers. Hence, the tilts of the $CoO_6$ octahedra should decrease (as observed; cf. the Co–O–Co bond angles in Table 3). This frequently results in stabilization of the rhombohedral $LaAlO_3$-type structure. However, for $Pr_{1-x}Sr_xCoO_{3-\delta}$ a different type of deformation is obtained.

For $x = 0$ and 0.20 the individual Co–O distances are of very similar length. However, from refinements without any distance soft constraints for $x = 0.50$, a larger spread in Co–O distances is found (Table 3) and the two different cobalt positions exhibit different average Co–O distances. This may indicate partial CO on Co. Bond-valence calculations show a valence difference of some 0.2 (10–295 K; Table 3). The bond-valence difference becomes slightly smaller at low temperature, but more important is the rearrangement from Co(1) to Co(2). This approach fails to reproduce the expected valence for cobalt according to the analytically established formula, the average Co bond valence being too large for $x = 0$ and 0.20 and too small for $x = 0.50$. Hence, the calculated compositional variation of the Co bond-valence is too narrow. The common root of these shortcomings is probably incorrectnesses in the available bond-strength parameters (20).

The coordination and bond distances for Co(1) in $x = 0.50$ at 10–295 K are very similar to the situation in $PrCoO_3$ ($Co^{3+}d^6$ LS). However, for Co(2), which possibly could reflect $Co^{4+}d^5$ HS, one would not expect a deformed octahedral coordination of the 4 + 2 type described in Table 3. This opens questions with regard to the reliability of the refined structure model with respect to the quality of the diffraction data.

To further approach the interesting question concerning possible CO, the introduction of strong distance soft constraints were considered an important remedy to come around the pseudo-cubic metric of the lattice and the consequent marked overlap of reflections in the PND profiles. The Co–O distances were soft constrained both with either one common Co–O distance for all cobalt atoms or with one common Co–O distance for each cobalt position. Both kinds of soft constraints resulted in significantly increased $R_p$ factors (Table 4). Although the present data could be

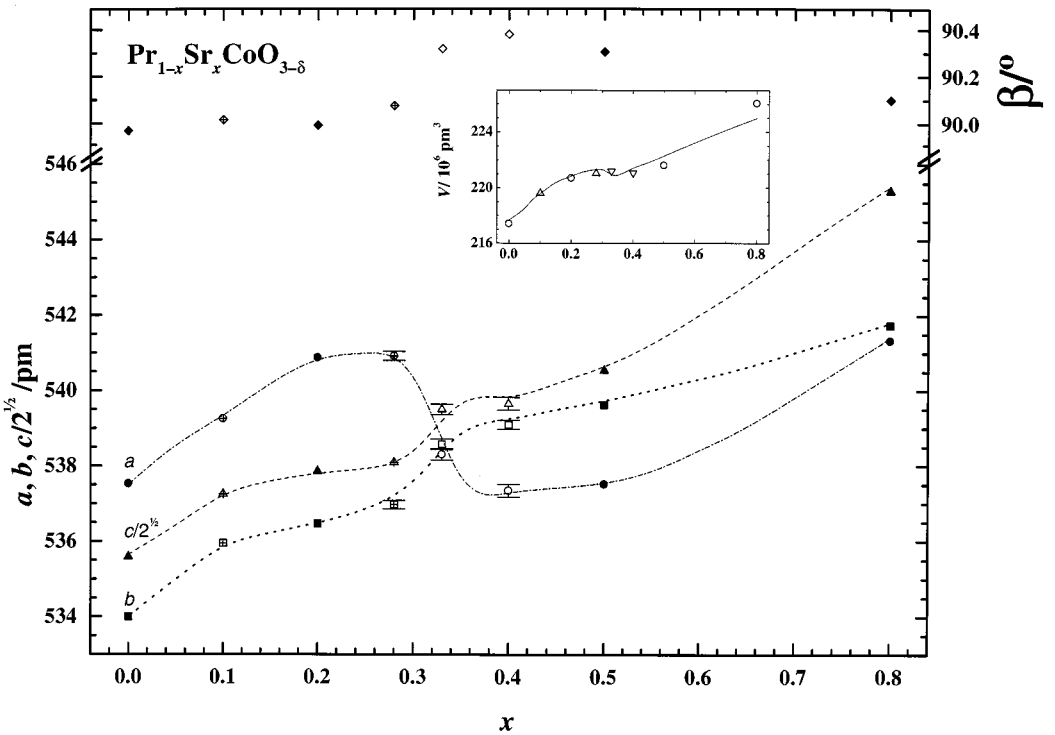


**FIG. 4.** Unit-cell dimensions according to a $P2_1/n$ description ($a$, circles; $b$, squares; $c/\sqrt{2}$, triangles; $\beta$, diamonds) for $Pr_{1-x}Sr_xCoO_{3-\delta}$ as a function of $x$ determined by Rietveld refinements of PND data (filled symbols), Rietveld refinements of PXD data (open symbols), and unit-cell refinements of peak positions with UNITCELL (crossed symbols). Curves are guides for eye. Inset: Unit-cell volume for $Pr_{1-x}Sr_xCoO_{3-\delta}$ as a function of $x$ (symbols) compared with those from Fig. 1 (curve).

taken in support of partial CO for $x = 0.50$, there are arguments against it. Since the electric conductivity is reported to be of a metallic nature (1–3), it seems somewhat unlikely that CO should be present at 295 K. Furthermore, the charge difference according to the bond valence is of the same magnitude at 295 and 10 K, which in turn only would be compatible with a very high CO temperature. This aspect will be discussed later.

### (*iii*) *Thermal Properties and Redox Behavior*

The oxygen content was analyzed by redox titrations and the results are presented in Fig. 5. For samples prepared in air at 900°C, the oxygen content shows almost no variation across the composition range where the most pronounced changes occur in the diffraction patterns. The crossover from *Pnma* to $P2_1/n$ symmetry is hence not connected with a change in the oxygen content. The oxygen vacancy concentration is almost negligable for $x < 0.50$. For $x = 0.24$ and 0.28, DSC shows a small endothermic peak at $\sim 230$°C. High-temperature PXD shows that there occurs a large change in the unit cell between 250 and 280°C, manifested in an enhanced difference in size between the axes. These thermal effects probably correspond to the changes in the electronic properties and crystal structure, which is observed at around $x = 0.30$ as a function of composition at room temperature (*vide infra and supra*).

When the Sr content is increased, $0 < x < 0.50$, one observes for samples prepared in air at 900°C that the charge imbalance is mainly ($\sim 85\%$) compensated by oxidation (formally) of $Co^{3+}$ to $Co^{4+}$; see inset to Fig. 5. The valence saturation for cobalt at $+3.4$ for samples prepared in air at 900°C appears not to reflect a fundamental aspect but rather to result from a trivial competition between two charge balance mechanisms with different temperature and oxygen partial pressure dependencies. The latter point is emphasized by the quite different situation found at higher temperatures, whereas seen from inset to Fig. 6 the overall stoichiometry at 1000°C can almost entirely be accounted for by oxygen vacancies.

An idea about the redox behavior throughout the $Pr_{1-x}Sr_xCoO_{3-\delta}$ solid-solution range is obtained by considering the compositional dependency of the change in the oxygen content between room temperature and 1000°C. A considerable reduction is then revealed. Figure 6 shows the weight difference as recorded by TG (here given in terms of $\Delta\delta$) for $0.10 \leq x \leq 0.80$. The oxygen loss reaches a maximum of 0.22 oxygen per formula unit for $x = 0.667$. The TG curves are smooth with no indications of (stable) intermediates. It is seen from Fig. 6 that the formal cobalt

**TABLE 3**
**Selected Distances (in pm) and Angles (°) Resulting from Rietveld Refinements of PND Data of $Pr_{1-x}Sr_xCoO_{3-\delta}$**

| $x$, $T$ (K) | 0, 295 | 0.20, 295 | 0.20, 10 | 0.50, 295 | 0.50, 170 | 0,50, 10 |
|---|---|---|---|---|---|---|
| Co′–O′ | 192.8 | 192.8 | 192.4 | 194.0 | 193.7 | 192.1 |
| Co″–O′ | | | | 188.8 | 187.5 | 188.9 |
| Co′–O″ | 192.9 | 193.1 | 192.3 | 190.1 | 190.7 | 192.9 |
| Co″–O″ | | | | 191.1 | 189.9 | 186.3 |
| Co′–O‴ | 192.9 | 192.9 | 193.0 | 196.1 | 193.6 | 184.5 |
| Co″–O‴ | | | | 190.3 | 192.3 | 202.6 |
| Pr/Sr–O | 235.6 | 240.2 | 237.5 | 287.0 | 287.5 | 282.7 |
| | 238.0 | 242.9 | 241.8 | 273.1 | 272.5 | 272.8 |
| | 238.0 | 242.9 | 241.8 | 274.6 | 275.4 | 278.1 |
| | 252.1 | 257.6 | 255.5 | 273.6 | 274.7 | 273.8 |
| | 258.9 | 260.9 | 260.4 | 286.9 | 285.0 | 290.8 |
| | 258.9 | 260.9 | 260.4 | 283.9 | 287.8 | 280.8 |
| | 267.3 | 270.7 | 268.7 | 254.6 | 252.2 | 255.9 |
| | 267.3 | 270.7 | 268.7 | 250.5 | 253.3 | 245.1 |
| | 287.5 | 283.2 | 284.2 | 271.5 | 268.8 | 269.7 |
| | 303.1 | 301.3 | 302.8 | 250.5 | 249.1 | 253.1 |
| | 313.2 | 306.1 | 306.5 | 269.7 | 264.8 | 265.6 |
| | 313.2 | 306.1 | 306.5 | 268.2 | 265.0 | 269.2 |
| Co′–O′–Co″ | 158.2 | 161.5 | 160.9 | 168.8 | 171.2 | 168.7 |
| Co′–O″–Co″ | | | | 176.1 | 173.6 | 177.3 |
| Co′–O‴–Co″ | 158.2 | 160.6 | 159.6 | 163.6 | 163.1 | 163.0 |
| $CN_{Pr/Sr}$ | 9 | 9 | 9 | 12 | 12 | 12 |
| $\bar{d}_{Pr/Sr-O}$ | 252.0 | 258.9 | 257.7 | 270.3 | 269.7 | 269.8 |
| $\bar{d}_{Co'-O}$ | 192.9 | 192.9 | 192.6 | 193.4 | 192.7 | 189.8 |
| $\bar{d}_{Co''-O}$ | | | | 190.1 | 189.9 | 192.6 |
| Valence Pr/Sr($CN_{Pr/Sr}$) | 2.928 | 2.766 | 2.873 | 2.675 | 2.734 | 2.724 |
| Valence Co′ | 3.234 | 3.228 | 3.261 | 3.195 | 3.254 | 3.529 |
| Valence Co″ | | | | 3.489 | 3.509 | 3.316 |

*Note*. Notations in $P2_1/n$: O′ = O(1), O″ = O(2), O‴ = O(2), Co′ = Co(1), Co″ = Co(2). *Pnma*: O′ = O″ = O(2), O‴ = O(1), Co′ = Co″ = Co.

valence at 1000°C in $O_2$ is close to 3. For samples most susceptible to reduction ($x > 0.50$, with large $\Delta\delta$ in Fig. 6), there are noticeable distinctions in oxygen content already between pure oxygen ($pO_2 = 1$ bar) and air (0.21 bar); 2.908 vs 2.874 for $x = 0.67$ and 2.883 vs 2.807 for $x = 0.80$ (referring to samples cooled to room temperature). The temperature required for establishing oxygen transport (as seen from the weight changes by TG) decreases with increasing $x$ from 600°C for $x = 0$ to 200°C for $x = 0.80$. In nitrogen $Pr_{0.50}Sr_{0.50}CoO_{3-\delta}$ shows the onset of reduction at about 150°C, whereas reduced $Pr_{0.50}Sr_{0.50}CoO_{3-\delta}$ reoxidizes slowly in air already at room temperature.

Increased oxygen contents may be obtained by turning to high oxygen partial pressures. For the samples with $x > 0.50$ treated at 450°C in $pO_2 = 125$ bar (where oxygen vacancy formation is the dominating charge compensation mechanism), an increase in oxygen content was observed (by TG) for $x = 0.667$, but not for $x = 0.80$ (compared to $pO_2 = 1$ bar). For the sample with $x = 0.50$, the unit-cell dimensions were not significantly altered, which indicates that for this sample oxygen saturation is closely obtained after heat treatment in air. For the samples with $0.24 \leq x \leq 0.35$ four extra reflections observed by PXD could be identified as a secondary cubic phase with $a = 426.7$ pm, thus matching the unit-cell dimension of CoO. Presence of CoO seems to be rather daring under these synthesis conditions, but nevertheless similar findings were also reported by others under very oxidative conditions (21, 22). Matsumoto *et al.* (22) suggested that electrochemical oxidation in a basic solution can lead to oxidation of water by $SrCoO_{3.00}$, which results in CoO at the surface. An analogous reaction can well take place between the high valent cobalt in the present samples and the water of the surrounding atmosphere or adsorbed water on the oxide. The resulting $OH^-$ could react with $Pr^{3+}$ and $Sr^{2+}$ to form amorphous hydroxides. The sample with $x = 0.24$ was investigated by means of scanning electron microscopy, but the particle size was found to be too small for a search for such products by EDX analysis.

### (*iv*) *Magnetic Properties*

The inverse magnetic susceptibility for $PrCoO_3$ (Fig. 7) shows paramagnetic behavior down to 5 K. This is in accordance with earlier findings for $RECoO_3$ perovskites with $Co^{3+}$ LS species in octahedral sites (23). There are nevertheless distinct features in $\chi^{-1}(T)$ for $Pr_{1-x}Sr_xCoO_{3-\delta}$. For $x \leq 0.20$ ($\delta \leq 0.01$) the Curie–Weiss law is actually fulfilled in two temperature ranges. The deduced paramagnetic parameters for $Pr_{1-x}Sr_xCoO_{3-\delta}$ are given in Table 5 where they are compared with different values for the

**TABLE 4**
**Reliablity Factor $R_p$ (%) for Rietveld Refinements of $Pr_{0.50}Sr_{0.50}CoO_{2.965}$ with and without Co–O Distance Restraints (The Standard Deviation Is Used in the Refinement To Establish the Weighting Factor)**

| | | $R_p$ | |
|---|---|---|---|
| $T$ (K) | Standard deviation | All Co–O equal | All Co–O equal on each Co site |
| 10 | No restriction | 7.2 | 7.2 |
| | 0.03 | 7.9 | 8.0 |
| | 0.025 | 9.3 | 9.6 |
| | 0.02 | 15 | 18 |
| 170 | No restriction | 5.6 | 5.6 |
| | 0.03 | 6.6 | 6.1 |
| | 0.025 | 7.2 | 6.6 |
| | 0.02 | 9.8 | 8.7 |
| 295 | No restriction | 5.9 | 5.9 |
| | 0.03 | 7.7 | 7.7 |
| | 0.025 | 24 | 25 |
| | 0.02 | 24 | 24 |

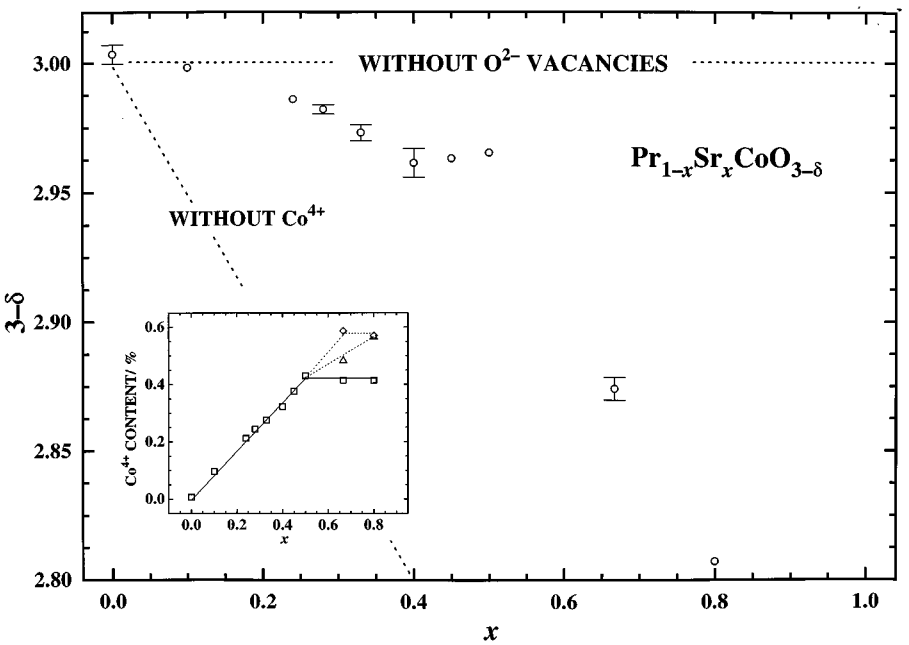


**FIG. 5.** Oxygen content for samples of $Pr_{1-x}Sr_xCoO_{3-\delta}$ prepared in air (circles). Inset: $Co^{4+}$ content for samples prepared in $pO_2 = 0.21$ bar (open squares), $pO_2 = 1$ bar (triangles), and $pO_2 \approx 125$ bar (diamonds).

paramagnetic moment under assumption of different possible spin states for $Co^{3+}$. In the calculations $Co^{4+}$ is assumed always to be in the HS state and $Pr^{3+}$ to take the $^3H_4$ electronic ground state. At low temperatures the results correspond fairly well to a LS state for $Co^{3+}$, while at elevated temperatures $\mu_p$ indicates HS $Co^{4+}$ for $x = 0$ and an intermediate spin [see, e.g., the findings for $LaCoO_3$(24)] for $x = 0.07$, 0.10, and 0.20.

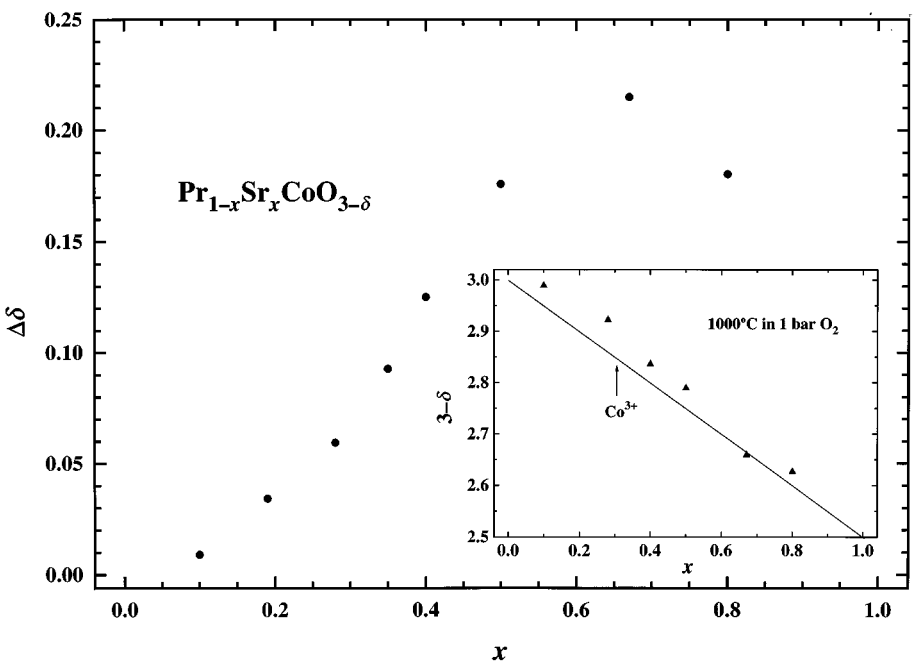


**FIG. 6.** Oxygen loss in $Pr_{1-x}Sr_xCoO_{3-\delta}$ obtained by heating to 1000°C in 1 bar $O_2$ (TG data). Inset: Oxygen content for $Pr_{1-x}Sr_xCoO_{3-\delta}$ at 1000°C in 1 bar $O_2$.

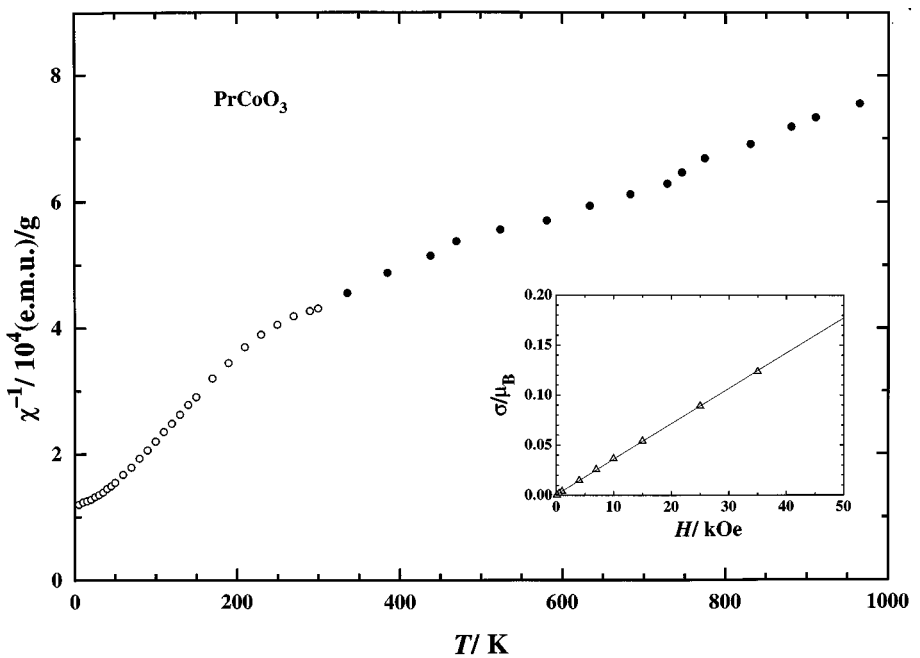


**FIG. 7.** Temperature dependence of inverse magnetic susceptibility for $PrCoO_3$ determined by SQUID (open circles) and Faraday measurements (filled circles). Inset: Field scan at 5 K.

Also, for $0.28 \leq x \leq 0.80$ the Cuire–Weiss law seems to be fulfilled at temperatures above $T_C$, but with our present SQUID setup, the paramagnetic state could only be followed in a very narrow temperature range, and a larger uncertainty is consequently attached to the derived values for $\mu_p$ and $\theta_p$. For $x > 0.50$ calculations of model values for the moments (according to our simple ionic picture) also become more difficult owing to the significant amount of oxygen vacancies, implying nonoctahedral coordination for a significant amount of the cobalt atoms. Nevertheless, it seems clear that the observed $\mu_p$ values are well below the predictions of all models in Table 5, which in turn suggest a delocalized model for the electronic structure.

Samples with $0.10 \leq x \leq 0.80$ show hysteresis behavior at 5 K (inset to Fig. 8). The magnetization is not saturated even at 45 kOe, which certainly reflects the paramagnetic contribution from $Pr^{3+}$. FC samples (from 300 to 5 K in a 45-kOe field) exhibit typical ferromagnetic behavior, whereas ZFC samples show a magnetization with a maximum at a temperature well below $T_C$ (Fig. 8). FC and ZFC magnetization curves merge at approximately 170 K for $0.28 \leq x \leq 0.80$ (lower temperatures for smaller $x$ in the range). The difference in the magnetization behavior between the FC and ZFC samples reflects the energy involved in the alignment of magnetic domains in $Pr_{1-x}Sr_xCoO_{3-\delta}$. $Pr_{1-x}Sr_xCoO_{3-\delta}$ is a relatively hard magnetic material (with a coercive field of 1.2 kOe for $x = 0.50$ at 5 K; inset to Fig. 8), and the applied measuring field (1 kOe) for the ZFC series is therefore not sufficient to align the domains alone. However, the thermal movements of the moments assist the alignment process and cause the magnetization to increase with increasing temperature up to the mentioned maximum. Even FC in 1 kOe proved to be sufficient to align the domains in $Pr_{0.50}Sr_{0.50}CoO_{2.965}$, giving a magnetization which only

**TABLE 5**

**Paramagnetic Moment ($\mu_p$) and Curie Temperature ($\theta_p$) for $Pr_{1-x}Sr_xCoO_{3-\delta}$ in the Indicated Temperature Regions Are Shown with Standard Deviations. ($\mu_p$ Is Compared with Three Spin Configuration Models (According to spin-only Assumption for Co): I, All $Co^{3+}$ in LS State and All $Co^{4+}$ in HS State; II, $Co^{3+}$ in Intermediate Spin and $Co^{4+}$ in HS; III, $Co^{3+}$ in HS and $Co^{4+}$ in HS)**

| $x$ | $T$ (K) | Exp. $\mu_p/\mu_B$ | Exp. $\theta_p$(K) | I, $\mu_p/\mu_B$ | II, $\mu_p/\mu_B$ | III, $\mu_p/\mu_B$ |
|---|---|---|---|---|---|---|
| 0.00 | 60–190 | 3.795(9) | − 58.3(6) | 3.578 | 4.561 | 6.066 |
| | 580–970 | 6.344(9) | − 537(21) | 3.578 | 4.561 | 6.066 |
| 0.07 | 100–175 | 3.74(1) | − 2.4(8) | 3.789 | 4.668 | 6.056 |
| | 235–270 | 4.75(4) | − 132(5) | 3.789 | 4.668 | 6.056 |
| 0.10 | 135–210 | 3.567(7) | 54.6(7) | 3.867 | 4.708 | 6.050 |
| | 260–300 | 4.69(3) | − 70(3) | 3.867 | 4.708 | 6.050 |
| 0.20 | 135–230 | 3.821(7) | 116.6(8) | 4.067 | 4.806 | 6.018 |
| | 270–300 | 4.47(4) | 68(5) | 4.067 | 4.806 | 6.018 |
| 0.28 | 260–300 | 3.60(3) | 188(6) | 4.214 | 4.879 | 5.992 |
| 0.30 | 260–300 | 3.44(3) | 206(5) | 4.250 | 4.897 | 5.985 |
| 0.40 | 245–300 | 3.50(1) | 238(2) | 4.361 | 4.942 | 5.937 |
| 0.50 | 245–300 | 3.85(2) | 235(3) | 4.631 | 5.100 | 5.927 |
| 0.67 | 245–300 | 3.13(2) | 236(4) | 4.317 | 4.833 | 5.726 |
| 0.80 | 215–300 | 3.176(7) | 199(2) | 4.121 | 4.656 | 5.576 |

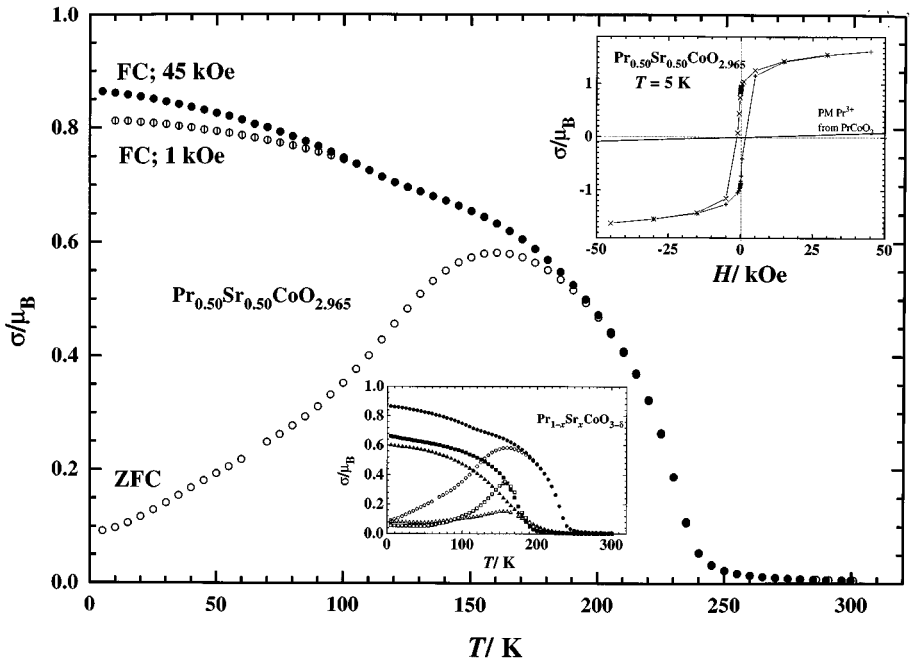


**FIG. 8.** Magnetization vs temperature curves for $Pr_{0.50}Sr_{0.50}CoO_{2.965}$ after FC and ZFC. Upper inset: Hysteresis at 5 K after FC. Lower inset: Magnetization after FC and ZFC for $x = 0.28$ (triangles), $x = 0.50$ (circles), and $x = 0.80$ (squares).

was slightly lower at 5 K than FC in 45 kOe (Fig. 8). Hence, close to $T_C$ the coercive field is of the order of the measuring field. An applied field of 45 kOe at 5 K is sufficient to align the domains in a ZFC sample.

The PND data for $x = 0.20$ and 0.50 are consistent with a ferromagnetic state at low temperatures. From Rietveld analysis ordered magnetic moments were derived, respectively 0.85(3) for $x = 0.20$ at 10 K and 1.44(10) and 1.12(10) $\mu_B$ for $x = 0.50$ at 10 and 170 K. These values correspond closely to the magnetization values at 45 kOe after correction for the paramagnetic contribution from $Pr^{3+}$: 0.78 $\mu_B$ ($x = 0.20$, 5 K), 1.55 $\mu_B$ ($x = 0.50$, 5 K), and 1.11 $\mu_B$ ($x = 0.50$, 160 K).

The direction of the ordered moment could not be established owing to the pseudo-cubic metric of the structure and the consequently strongly overlapping magnetic reflections. However, it is plausible that the large change in $c$ for $Pr_{0.50}Sr_{0.50}CoO_{2.965}$ between 10 and 170 K reflects magnetostriction and perhaps indicates that the moment is aligned along $c$. No similar anomaly was observed for the weakly ferromagnetic $Pr_{0.80}Sr_{0.20}CoO_{2.99}$ sample.

The compositional dependencies of $T_C$ and the saturation moment of Co at 5 K and 45 kOe are shown in Fig. 9. $T_C$ and $\sigma_{Co}$ are clearly functions both of the formal cobalt oxidation state (the $Co^{4+}/Co^{3+}$ ratio) and the oxygen content (the local coordination around Co). In Fig. 10 one of these parameters has been varied at the time while the other has been kept constant. Increasing $Co^{4+}$ content increases $T_C$ and $\sigma_{Co}$, while increasing oxygen nonstoichiometry decreases $\sigma_{Co}$ and to a certain extent also $T_C$. The expected decrease in magnetization and ordering temperature for samples with $x = 0.50$, which after reduction by TG immediately had been subjected to magnetization measurements, is illustrated in Fig. 11.

## IV. DISCUSSION

The existence range of the $Pr_{1-x}Sr_xCoO_{3-\delta}$ solid-solution phase can be considered to be bracketed between two extreme oxygen contents: One with $\delta = 0$, i.e., with no oxygen vacancies and a linearly increasing amount of $Co^{4+}$ (formally $Pr_{1-x}Sr_xCo^{3+}_{1-x}Co^{4+}_xO_3$) as the charge compensation for the aliovalent substitution; the other with $\delta = x/2$, i.e., $Pr_{1-x}Sr_xCo^{3+}O_{3-x/2}$ with oxygen vacancies as the charge compensation mechanism. In the former case, all cobalt atoms remain in octahedral coordination. In the latter, defect octahedra of various kinds will exist locally, probably mostly in the form of square pyramids and tetrahedra.

The charge compensation mechanism is strongly dependent on temperature and oxygen partial pressure used under synthesis or during property measurements (assuming equilibrium). Hence, this is another aspect of the oxygen nonstoichiometry in such phases. For $x \leq 0.50$ one observes for samples prepared in air a mixture of formally cobalt $Co^{3+}$ and $Co^{4+}$ with negligible amounts of oxygen

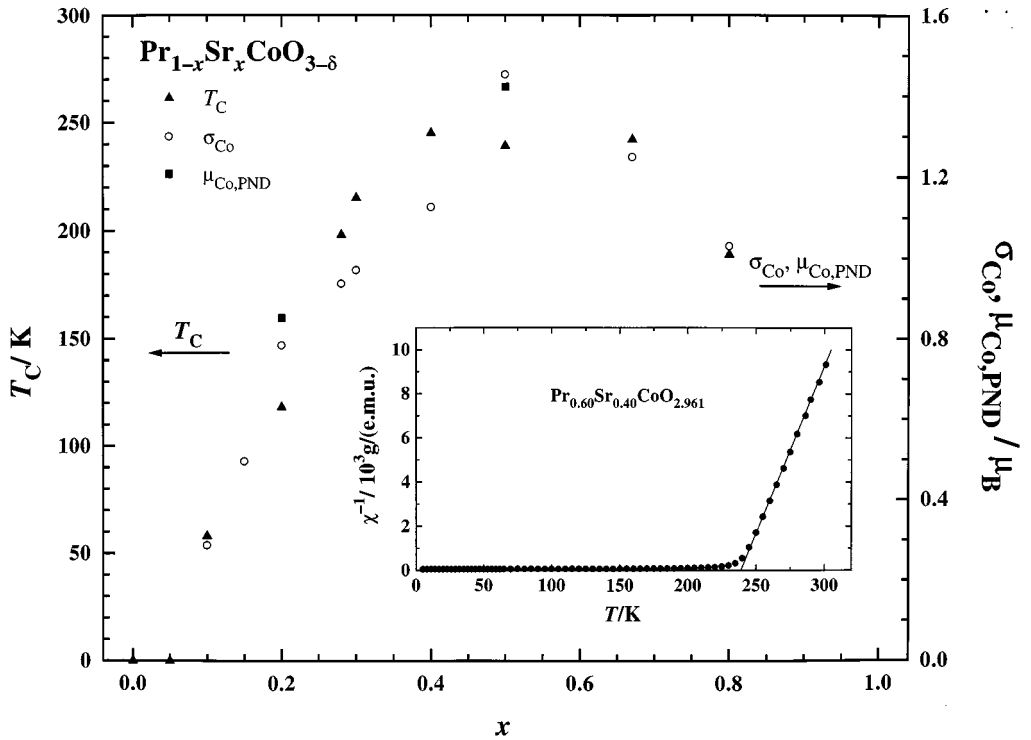


**FIG. 9.** $T_C$ and $\sigma_{Co}$ (45 kOe, 5 K) for ZFC samples of $Pr_{1-x}Sr_xCoO_{3-\delta}$. Inset: $\chi^{-1}(T)$ for $Pr_{0.60}Sr_{0.40}CoO_{2.961}$.

vacancies. However, for enhanced substitution levels $x > 0.50$ the additional charge imbalance is compensated by oxygen vacancies (Fig. 5).

The described situation is of a general nature for perovskite-type oxides; however, the delicate balance is more visible for the heavier 3*d* elements. There are at least two

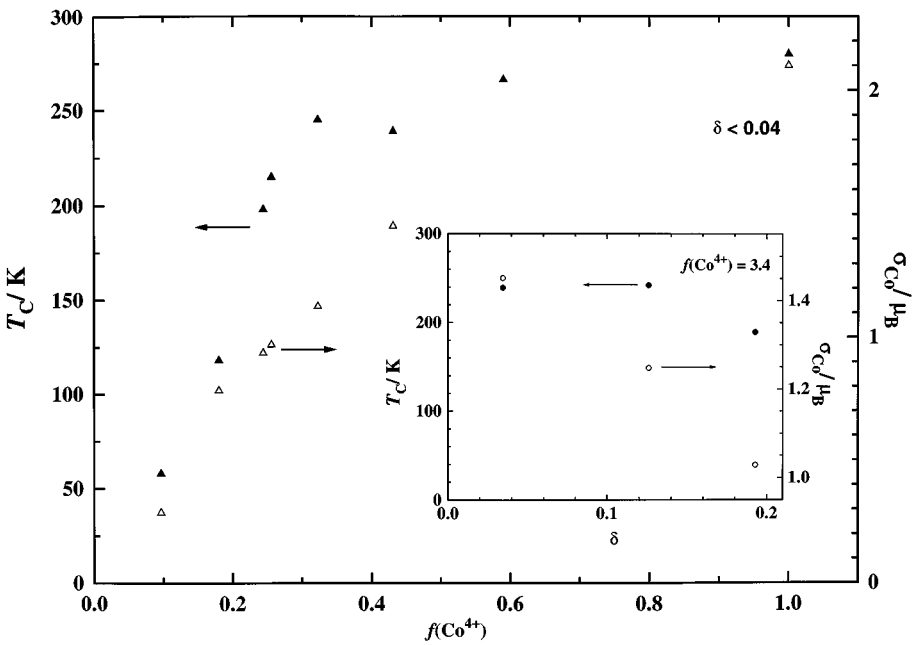


**FIG. 10.** $T_C$ (filled symbols) and $\sigma_{Co}$ (open symbols) for $Pr_{1-x}Sr_xCoO_{3-\delta}$ as a function of $Co^{4+}$ content [$f(Co^{4+})$] for samples with approximately constant $\delta$ (different $x$). Data for sample with $f(Co^{4+}) = 1$ is taken from Ref. 21. Inset: $T_C$ (filled symbols) and $\sigma_{Co}$ (open symbols) for $Pr_{1-x}Sr_xCoO_{3-\delta}$ as a function of oxygen nonstoichiometry $\delta$ for samples with approximately the same $Co^{4+}$ content.

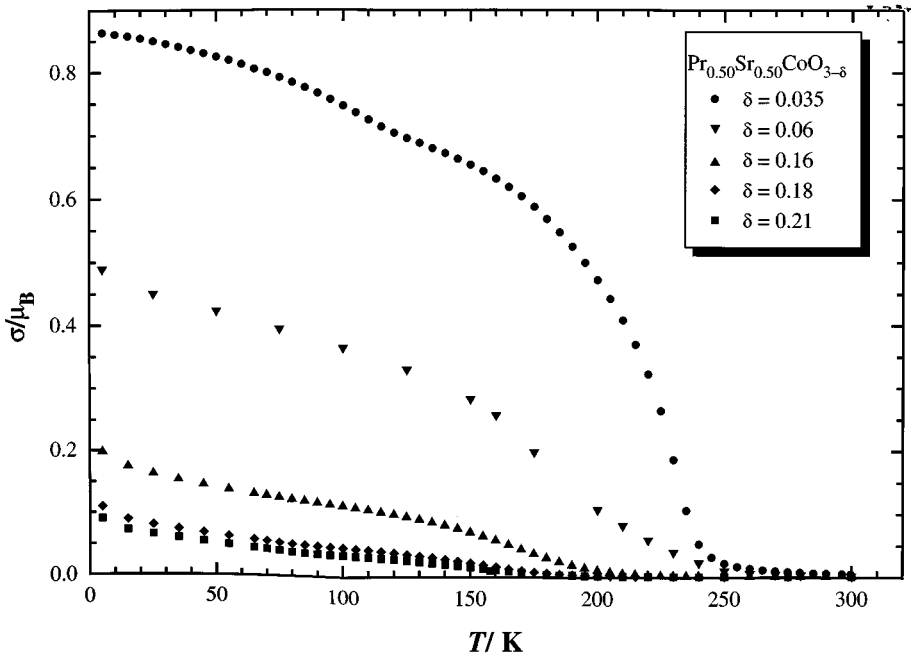


**FIG. 11.** Magnetic susceptibility of reduced $Pr_{0.50}Sr_{0.50}Co_{3-\delta}$ samples. Legend to $\delta$ is given on the illustration.

main reasons for this situation; the perovskite structure can easily (topochemically) adjust to large oxygen defect concentrations by locally introducing other coordination polyhedra than octahedra, and the ionization potentials for the higher oxidation states increases on increasing the effective nuclear charge throughout the 3*d* series. One may therefore envisage that stabilization from oxygen vacancy formation becomes increasingly important. The present results for $x \leq 0.50$ suggest a vacancy concentration of $\delta \leq 0.04$ for samples prepared in air, even though Co oxidation is the main charge-balancing mechanism.

With respect to the size of the cations, one may speculate whether the oxidized $Co^{4+}$ would be too small to be accommodated for in a perovskite-type structure. LS $Co^{4+}$ would most probably be too small, according to, say, the Goldschmidt criterion, for the formation of stable $BO_6$ octahedra. Based on Shannons radii (25) even LS $Co^{3+}$, and hence also the slightly smaller HS $Co^{4+}$, should have a too small size, but such perovskite-type oxides are nevertheless known. Electron spectroscopy data for the related $La_{1-x}Sr_xCoO_{3-\delta}$ show that the HS state for $Co^{4+}$ is around 1 eV lower in energy than the LS state (26). It is reasonable to assume that this also holds for $Pr_{1-x}Sr_xCoO_{3-\delta}$.

In the magnetic susceptibility data for $Pr_{1-x}Sr_xCoO_3$ praseodymium gives a paramagnetic contribution in the measured temperature interval ($T > 5$ K), whereas cobalt is dia-, para-, or ferromagnetic, depending on the composition and temperature. For $x = 0$ cobalt is in an LS state at 5 K and is hence diamagnetic. On substitution of $Pr^{3+}$ by $Sr^{2+}$, $Co^{3+}$ is partially oxidized to $Co^{4+}$, which carries a magnetic moment. For small concentrations of $Co^{4+}$, it is reasonable to assume that the material remains paramagnetic down to 5 K, but already for $x = 0.05$ the magnetization–field curve at 5 K is nonlinear, and for $x = 0.10$, hysteresis is definitively established. For $x = 0.20$ long-range ferromagnetic order is proved by PND. The indications of ferromagnetic-like behavior in the magnetization curves for samples with lower values of $x$ may reflect the formation of spin clusterglass, which is claimed to be the case for $La_{1-x}Sr_xCoO_3$ with small $x$ (6, 27).

For $Pr_{0.80}Sr_{0.20}CoO_{2.99}$ with 17% HS $Co^{4+}$ and 83% LS $Co^{3+}$, one would expect an ordered magnetic moment of 0.85 $\mu_B$ per Co atom (assuming a spin-only situation for cobalt). This is consistent with 0.85(3) $\mu_B$ obtained by PND at 10 K and 0.78 $\mu_B$ found by magnetization measurements at 5 K. Correspondingly, one would expect a moment of 2.15 $\mu_B$ per Co atom for $Pr_{0.50}Sr_{0.50}CoO_{2.965}$, which however, is considerably higher than the observed ordered moments by PND (1.42(10) $\mu_B$ at 10 K) and magnetization measurements (1.55 $\mu_B$ at 5 K). This discrepancy indicates a change in electronic properties, which probably is connected with the structural transition around $x \approx 0.30$, and would furthermore be consistent with the reported semiconductor-to-metal transition at $x \approx 0.25$ (1–3). The significant reduction of $\sigma_{Co}$ for $x > 0.30$ falls in line with the observed reduced moment of 2.15 $\mu_B$ for $SrCoO_3$ (21), compared to the expected moment of 5 $\mu_B$ within this model. In addition,

one should not forget the possibility that $Pr_{0.50}Sr_{0.50}CoO_{2.965}$ may contain less $Co^{4+}$ than expected, owing to the possible oxidation of $Pr^{3+}$ or $O^{2-}$.

It is reported that the temperature derivative of the resistivity changes sign between $x = 0.20$ and 0.30 at room temperature (1–3). This semiconductor-to-metal transition is probably intimately related to the structural change observed in the present study at $x \approx 0.30$ at room temperature. Our preliminary study of a sample with $x = 0.24$ by high-temperature PXD has revealed a structural transition between 250 and 280°C. This may well be a point on the composition vs temperature characteristics of the same transition. Kostogloudis *et al.* (3) observed the semiconductor-to-metal transition at 500°C for $x = 0.15$, but were unable to detect it up to 800°C for $x = 0$. Hence, the semiconductor region at low temperature and low substitution levels is surrounded by a region with metallic conductivity. The change in conductivity appears consistent with the observed increase in the Co–O–Co bond angles between the *Pnma* and $P2_1/n$ structure regimes, since these angles characterizing the octahedral tilts are important for the $\pi$ overlap between O(2*p*) and Co(3*d*) ($t_{2g}$) orbitals.

Ferromagnetism appears to be characteristic of $RE_{1-x}A_xCoO_3$ with divalent substituents on the RE sublattice. A double-exchange mechanism has been suggested as an explanation for the coexistence of ferromagnetism and metallic conductivity in corresponding $Mn^{3+}/Mn^{4+}$ perovskites (28). Whether double exchange also prevails for the $Co^{3+}/Co^{4+}$ perovskites is not clear at present (6).

Since the Glazer symmetry considerations for single perovskites are not compatible with the present diffraction data for $Pr_{0.50}Sr_{0.50}CoO_{2.965}$, an alternative structure model with two Co sites was chosen (disregarding the unlikely possibility of phase segregation into closely related perovskite superstructural phases). From the derived crystal data, bond-valence calculations resulted in a valence difference between the two Co sites of approximately 0.2. This difference suggests that a chemical reason for the symmetry reduction could be a partial charge ordering (CO) for $x \approx 0.50$. This hypothesis has support in stability calculations which predict an energy gain by CO on the *B* position in perovskites (29). CO is well documented for perovskites with manganese in the *B* position, e.g., $La_{0.50}Ca_{0.50}MnO_3$ (30) and $Nd_{0.50}Ca_{0.50}MnO_3$ (31). In the manganese perovskites, the CO is associated with a large change in unit-cell dimensions resulting from cooperative Jahn–Teller distortion of $Mn^{3+}$ and is therefore quite easy to detect. For the Co perovskites any CO phenomenon would probably be more difficult to observe ($d^6$ LS, $d^5$ HS).

To our knowledge CO is not documented for any regular Co perovskite. In addition, if the electronic conductivity, which is known to be of the metallic kind, is substantial, one would expect that any tendency toward CO should be efficiently counteracted. Furthermore, the calculated bond–valence difference between the two Co sites is of the same magnitude at 10 and 295 K, which in turn predicts a rather high CO temperature on the assumption that the transition is second order. In the manganese perovskites this transition occurs well below room temperature. It is also interesting in this connection to pay attention to Kumar *et al.* (31) who report a bond-valence difference of ca. 0.15 between the Mn sites in $Na_{0.50}Ca_{0.50}MnO_3$ *above* the CO temperature. The open question is then if bond-valence differences of this size are significant or just consequences of overoptimistic confidence in refinement results extracted from data which are not of matching quality. An additional complicating factor enters when one recalls that X-ray absorption near-edge spectroscopy data for $La_{1-x}Sr_xCoO_3$ suggest that at least part of the oxidation of this phase may be realized by holes in bands of strong oxygen character rather than to specific valence changes on Co (32). Within this unclear picture it is no trivial task to conclude on possible CO in $Pr_{1-x}Sr_xCoO_3$ for $x \approx 0.50$, but the possibility can, however, not be ruled out.

## ACKNOWLEDGMENT

H.W.B. is grateful to The Research Council of Norway for financial support.

## REFERENCES

1. C. N. R. Rao and O. Parkash, *Philos. Mag.* **35,** 1111 (1977).
2. V. V. Kharton and A. K. Demin, *Inorg. Mater.* **29,** 217 (1993).
3. G. Ch. Kostogloudis, N. Vasilakos, and Ch. Ftikos, *Solid State Ionics* **106,** 207 (1998).
4. H. Ohbayashi, T. Kudo, and T. Gejo, *Jpn. J. Appl. Phys.* **13,** 1 (1974).
5. R. Mahendiran, A. K. Raychaudhuri, A. Chainani, and D. D Sarma, *J. Phys.: Condens. Matter* **7,** L561 (1995).
6. R. Mahendiran and A. K. Raychaudhuri, *Phys Rev. B* **54,** 54 (1996).
7. R. Mahendiran, A. K. Raychaudhuri, A. Chainani, and D. D. Sarma, *Rev. Sci. Instrum.* **66,** 3071 (1995).
8. N. Itoh, T. Kato, K. Uchida, and K. Haraya, *J. Membr. Sci.* **92,** 239 (1994).
9. V. V. Kharton, E. N. Naumovich, and A. V. Nikolaev, *J. Membr. Sci.* **111,** 149 (1996).
10. C. B. Zehn, T. R. Ling, and M. D. Lee, *React. Kinet. Catal. Lett.* **62,** 185 (1997).
11. Y. Wu, T. Yu, B. Dou, C. Wang, X. Xie, Z. Yu, S. Fan, Z. Fan, and L. Wang, *J. Catal.* **120,** 88 (1989).
12. B. Noläng, "Program UNITCELL," Version 0.9. Institute of Chemistry, University of Uppsala, Uppsala, Sweden, 1997.
13. K. Yvon, W. Jeitschko, and E. Parthé, *J. Appl. Crystallogr.* **10,** 73 (1977).
14. J. Rodriguez-Carvajal, "FULLPROF98," Version 0.2, ILL, Grenoble, France, 1998.
15. W. T. A. Harrison, S. L. Hegwood, and A. J. Jacobson, *J. Chem. Soc., Chem. Commun.* **19,** 1953 (1995).
16. A. M. Glazer, *Acta Crystallogr. A* **31,** 756 (1975).
17. P. M. Woodward, *Acta Crystallogr. B* **53,** 32 (1997).
18. F. A. Cotton and G. Wilkinson, "Advanced Inorganic Chemistry," 3rd ed. Interscience, New York, 1972.
19. D. Altermatt and I. D. Brown, *Acta Crystallogr. B* **41,** 240 (1985).
20. N. E. Brese and M. O'Keeffe, *Acta Crystallogr. B* **47,** 192 (1991).

21. P. Bezdicka, A. Wattiaux, J. C. Grenier, M. Pouchard, and P. Hagenmuller, *Z. Anorg. Allg. Chem.* **619,** 7 (1993).
22. Y. Matsumoto, H. Manabe, and E. Sato, *J. Electrochem. Soc.* **127,** 811 (1980).
23. W. H. Madhusudan, K. Jagannathan, P. Ganguly, and C. N. R. Rao, *J. Chem. Soc., Dalton Trans.* 1397 (1980).
24. S. Stølen, F. Grønvold, H. Brinks, T. Atake, and H. Mori, *Phys. Rev. B* **55,** 14103 (1997).
25. R. D. Shannon, *Acta Crystallogr. A* **32,** 751 (1976).
26. A. Chainani, M. Mathew, and D. D. Sarma, *Phys. Rev. B* **46,** 9976 (1992).
27. J. Mira, J. Rivas, R. D. Sanchez, M. A. Senaris-Rodriguez, D. Fiorani, D. Rinaldi, and R. Caciuffo, *J. Appl. Phys.* **81,** 5753 (1997).
28. R. Mahesh, R. Mahendiran, A. K. Raychaudhuri, and C. N. R. Rao, *J. Solid State Chem.* **120,** 204 (1995).
29. G. Hong, G. Bing-lin, and Z. Xiao-wen, *J. Am. Ceram. Soc.* **79,** 381 (1996).
30. P. E. Schiffer, A. P. Ramirez, W. Bao, and S.-W. Cheong, *Phys. Rev. Lett.* **75,** 3336 (1995).
31. N. Kumar and C. N. R. Rao, *J. Solid State Chem.* **129,** 363 (1997).
32. J. E. Sunstrom, K. V. Ramanujachary, and M. Greenblatt, *J. Solid State Chem.* **139,** 388 (1998).